Spectral Bandwidth and WEC Performance Assessment

J.-B. Saulnier[1], P. Ricci[2], M. T. Pontes[1] and A. F. de O. Falcão[2]

[1] Department Renewable Energies, Instituto Nacional de Engenharia, Tecnologia e Inovação
Estrada do Paço do Lumiar, 1649-038 Lisboa, Portugal
E-mail: jbaptiste.saulnier@ineti.pt
E-mail: teresa.pontes@ineti.pt

[2] Department of Mechanical Engineering, Instituto Superior Técnico,
Av. Rovisco Pais 1049-001, Lisboa, Portugal
E-mail: pricci@hidro1.ist.utl.pt
E-mail: falcao@hidro1.ist.utl.pt

Abstract

This paper investigates the dependency of wave energy conversion on the spectral bandwidth of sea-states. To this aim, the performance of an axisymmetrical Wave Energy Converter is assessed in the frequency domain by using a stochastic model in two far different wave climates (Portugal and North Sea) both represented by more than 23000 energy spectral densities obtained from measurements. The correlation between the performance and various bandwidth parameters found in the literature is observed. Then, refined methods for predicting the long-term converted wave energy based on wave statistics including spectral bandwidth are compared to more common procedures and conclusions are drawn.

Keywords: Wave Energy Converter, Performance Assessment, Spectral Bandwidth, Stochastic Modelling.

Introduction

Assessing the performance of a Wave Energy Converter (WEC) – that is, predicting the effective amount of energy converted from the incident wave field over certain period of time in nominal operation conditions – necessarily requires a precise knowledge of the local wave climate. The developers, indeed, need to optimize their devices in order to fit them to actual wave conditions at the envisioned zone of deployment. The main wave characteristics are commonly given in terms wave height, period, direction of propagation and power. Then, representative sea-states of the local wave climate (energy spectra $E(f)$) are modelled using these parameters and input in numerical models or in wave-tank for experimental model testing. By multiplying the number of occurrences of such sea-states observed at sea to the corresponding extracted power output from the models, an estimation of the converted wave energy over a given period of time is easily derived. To date, most of WEC performance predictions are based on this procedure, using unimodal Pierson-Moskowitz / Bretschneider or JONSWAP [1] energy spectra to describe the representative sea-states.

Observations of spectra (frequency domain) obtained from measurements let suggest however that such models are not always realistic. Often, sea-states are not unimodal since they are the result of various wave systems (superimposed remotely originated swells and local wind-seas) leading to complex multimodal spectral shapes. Moreover, in case they can be considered as unimodal, the observed spectra may exhibit a wide variety of shape patterns. The missing information for an extensive sea-state characterisation is then the spectral bandwidth. Accordingly, the common prediction methods using shape-fixed analytical representative spectra may lead to some discrepancies with reality since the shape variations are never taken into account.

A single spectral parameter can certainly not distinguish whether the energy spectrum has one, two or more peaks. This identification would be anyway highly dependent on the accuracy of the spectral estimates, which in turn depends on the numerical procedures that have been performed beforehand to compute them. However, this information is not always useful for WEC designers, whose main concern is to tune their device to the most energetic frequency band of the wave field. If wave directionality does not significantly influence the device's response (which is the case for an axisymmetrical device) three wave parameters may therefore suffice to characterise the incoming wave energy in the frequency domain and characterise in turn the device performance: the mean wave height, period and spectral bandwidth.

A review of various spectral bandwidth parameters drawn from literature is first presented in this paper. Then a numerical code that stochastically models the wave energy conversion operated by an axissymetrical converter (IPS Buoy) in the frequency domain is used to compute the extracted wave power from a given energy spectrum $E(f)$, by four linear Power Take-Off (PTO) configurations. Two large samples of spectral measurements are input to the model, the first one being mostly related to North-Atlantic swell-dominated wave conditions (western coast of Portugal) and the other one to wind-waves (North Sea), which each include more than 23000 spectra. Each sea-state (spectrum) is characterised by its significant wave height H_{m0}, its mean energy period T_{-10} and the set of bandwidth parameters referred to above. The observed results on both wave climates are shown and some relevant conclusions for wave energy conversion purposes are formulated.

Lastly, refined methods for assessing the annual performance of the device involving in the wave statistics a spectral bandwidth parameter as a third degree of freedom

are implemented and compared to the classical one as well as to the exact values. Conclusions are then drawn for future works.

1 Sea-States Spectral Characterisation

A sea-state is defined as stationary wave conditions observed at a given point of the sea. The most basic data used to describe the sea-states are generally the significant wave height, mean period and direction of waves. However, a complete description of the sea-state in the frequency domain is possible by computing the energy spectrum (or spectral density) $E(f)$ from *in situ* measurements or wave predictive models, which gives the distribution of energy against frequency. Such data is widely available today and is sufficient to characterise sea-states when no wave directional information is needed.

The spectral moments at order n of the spectrum are computed as

$$m_n = \int_0^\infty f^n E(f) df \tag{1}$$

It is then possible to derive wave spectral parameters, such as the significant wave height

$$H_{m0} = 4\sqrt{m_0} \tag{2}$$

which is related to the wave energy level through the sea-surface elevation variance m_0, and the mean energy period

$$T_{-10} = \frac{m_{-1}}{m_0} \tag{3}$$

The wave power is computed as

$$P_w = \rho g \int_0^\infty c_g(f) E(f) df \tag{4}$$

where c_g denotes the wave group velocity, which depends on the water depth h (see e.g. [2] for its computation), ρ the sea water density (= 1025kg/m^3) and g the gravitational acceleration. Under infinite water depth assumptions (i.e. kh>>1 with k the wave number of the harmonic f) the wave power level simplifies to

$$P_w = \frac{\rho g^2}{64\pi} {H_{m0}}^2 T_{-10} = 0.4906 {H_{m0}}^2 T_{-10} \tag{5}$$

which is commonly expressed in kW/m of wave front if H_{m0} and T_{-10} are respectively expressed in meters and seconds.

To characterise the spectral bandwidth of a sea-state, several parameters are presented hereafter. Some of them were used to deal with wave groupiness as this phenomenon is known to be somehow linked to the spectral narrowness (the narrower the spectrum, the more grouped the waves).

Longuet-Higgins [3] introduced the narrowness parameter υ to study wave groups in narrow-banded random sea-states

$$\upsilon = \sqrt{\frac{m_0 m_2}{{m_1}^2} - 1} \tag{6}$$

As his theory was limited to the consideration of narrow spectra, he recommended imposing systematically low and high cut-off frequencies for its computation. However, it is here deliberately performed over the whole frequency band as the measured sea-states were not necessarily narrow-banded. For the sake of clarity this parameter is denoted by ε_2 in the following.

For wave energy resource assessment, Mollison [4] proposed the use of parameter ε_0 defined as

$$\varepsilon_0 = \sqrt{\frac{m_0 m_{-2}}{{m_{-1}}^2} - 1} \tag{7}$$

which is the relative standard deviation of the corresponding period spectrum. Smith [5] in turn used an intermediate bandwidth parameter ε_1, as

$$\varepsilon_1 = \sqrt{\frac{m_1 m_{-1}}{{m_0}^2} - 1} \tag{8}$$

The peakedness factor

$$Q_p = \frac{2}{{m_0}^2} \int_0^\infty f E^2(f) df \tag{9}$$

was introduced by Goda [6] and aims at characterising the sharpness of the spectral peak. Obviously, such a factor makes full sense for monopeaked spectra. Spectra whose $Q_p \sim 2$ correspond to wind-waves whereas $Q_p > 3 - 4$ rather characterises swells.

The wave height correlation parameter κ has been proposed by Battjes and Van Vledder [7] to study wave group characteristics. The correlation between two successive wave heights is logically related to the groupiness of waves indeed. It is calculated as

$$\kappa = \kappa(\tau) = \frac{1}{m_0} \cdot \left| \int_0^\infty E(f) \cdot e^{i 2\pi f \tau} df \right| \tag{10}$$

where the time-lag τ is usually taken equal to the mean zero up-crossing wave period $T_{02} = \sqrt{(m_0/m_2)}$.

Finally, a last spectral bandwidth parameter B_w [Prevosto, personal communication] is also included in this study, as

$$B_w = \frac{4}{{m_0}^2} \int_0^\infty E^2(f) \left(f - \frac{m_1}{m_0} \right)^2 df \tag{11}$$

By construction, this parameter has the particularity of not depending on the position of the spectrum in frequency, contrary to the previous ones.

Independently of their original use, all of these parameters are seen here as spectral shape or bandwidth factors, that is, the third missing degree of freedom for a comprehensive characterisation of sea-states. In the following sections, they are computed on real ocean energy spectra together with H_{m0} and T_{-10}.

2 Wave Data

Two western European different wave climates are used in this study (Fig. 1). They were obtained from long time-series of energy spectra calculated from 3-hourly buoy measurements. The first one is the swell-dominated climate off Portuguese western coast (Figueira da Foz, "FF"). The measurements were made at 40º13'33"N, 09º06'00"W by Wavec and Waverider buoys over nearly thirteen years (1981-1994) by the Portuguese Hydrographical Institute (*Instituto Hidrográfico*), the number of spectra totalling ca. 26500. The second one refers to the North Sea prevailing wind-waves conditions off the Dutch coasts ("K13"), at 53º12'17"N, 03º03'10"E. About 23300 measurements by Wavec buoys from 1993 to 2002 were provided by the Dutch National Institute for Marine and Coastal Management (*Rijkswaterstaat*). Deep water conditions can be assumed at FF as the water depth is ~90m. At K13 where the water depth is ~30m finite water depth assumptions must be adopted.

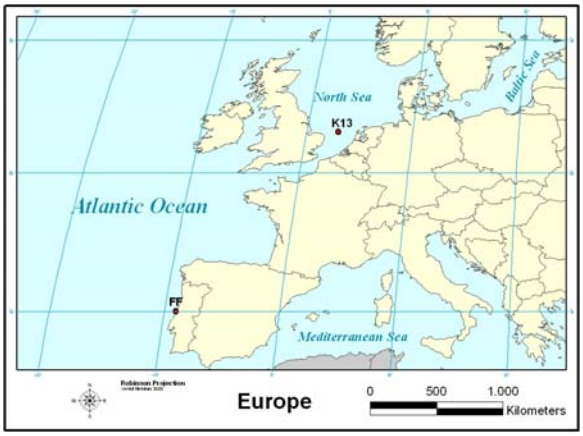

Figure 1: Buoy measurement sites; North Atlantic/Portugal (FF) and North Sea/Netherlands (K13).

The buoys suffered sporadic technical difficulties that led to data failures. Half-hour measurements were made during extreme sea-states (H_{m0} > 5m). However, the duration of both measurements campaigns is quite long (9 years min.), which enables to consider the available sets of spectral data as representative samples.

For the purposes of the study presented below, only the mostly observed sea-states with $T_{-10} \in$ [5s;15s] at FF and $T_{-10} \in$ [3s;10s] at K13 were kept, which slightly reduced the samples (to 25300 and 23000 spectra respectively).

Spectral sub-samples were formed by selecting spectra according to their mean energy period T_{-10}, resulting in 21 sub-samples with T_{-10} = {5s, 5.5s, … , 14.5s, 15s} for FF, and similarly 13 with T_{-10} = {3.5s, 4s, … , 9s, 9.5s} for K13, allowing a 2% margin on T_{-10}. Each spectral sub-sample never contained less than 50 elements.

The unique criterion of selection to build up these sub-samples is based on wave period T_{-10}. The justification of this is addressed in the next sections.

3 IPS Buoy WEC Stochastic Model

Different devices have been proposed to exploit the wave energy potential in the last years. Among them, the conception of the Wave Point Absorber, essentially based on an oscillating body, is one of the most promising technologies, particularly fit to offshore installations. In general, this kind of converters uses as PTO system either a hydraulic system or a directly driven linear electric generator.

A single oscillating rigid body is one of the earliest concepts of wave-energy device, for which some fundamental theoretical results were firstly derived by Evans [8]. An insight of the main concepts, including optimal power absorption conditions, was developed and systematised by Falnes [9]. These authors showed, in particular, that the maximum energy that may be absorbed by a heaving axisymmetrical body equals the wave energy transported by the incident wave along a front width equal to the wavelength divided by 2π. This upper limit may be achieved using an optimum control ("reactive control").

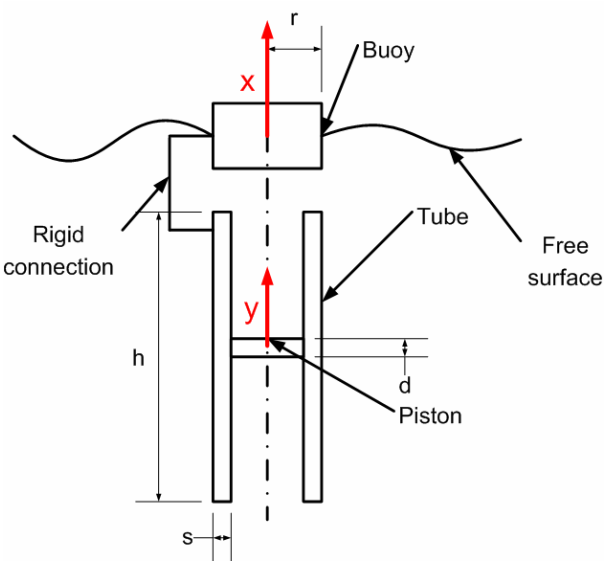

Figure 2: Simplified scheme of an IPS buoy.

Among the variety of devices that may be regarded as Point Absorbers, we consider here a system that consists of a fully submerged vertical open tube rigidly connected to a

floating buoy and a piston able to slide inside it (see [10]). Tube and buoy constitute therefore a single body subject to wave induced motions while the piston motion is mainly dominated by the water inertia inside the tube, providing in this way the desired reaction for the energy extraction. This conception, illustrated in Figure 2, is, in some way, similar to an IPS buoy, a device proposed and developed in the 1980s, which later evolved into the AquaBuOY™, a wave energy converter currently being developed by Finavera (www.finavera.com).

In the following we assume linear water wave theory, incompressible, inviscid fluid and irrotational flow. If we also consider a linear PTO system (ideally composed of a linear damper and a linear spring term), we may apply a frequency domain analysis and generate a Power Transfer Function (PTF) dependent on the frequency for each pair of PTO coefficients.

The assumption of a linear PTO allows us to perform a stochastic modelling in order to estimate the average power output corresponding to each sea-state, which will be characterized by its own energy spectrum. This method has been developed, for the case of the Oscillating Water Column, by Falcão and Rodrigues [11] and Falcão [12].

Basically we assume that each sea-state may be represented by a stochastic ergodic process, considering the surface elevation as a stochastic input. We then assume that each degree of freedom of the system could be considered as a random variable of zero mean, which is related to the surface elevation by the means of a transfer function.

In the present case, we consider two degrees of freedom, one (x) related to the buoy displacement and the other one (y) linked to the piston movement. We therefore consider the velocities as Gaussian distributions given by

$$\begin{aligned} \dot{x}(t) &= N(0,\sigma_{\dot{x}}) \\ \dot{y}(t) &= N(0,\sigma_{\dot{y}}) \end{aligned} \tag{12}$$

where σ indicates standard deviation. Since the instantaneous power is given by

$$P(t) = C_{PTO}\,(\dot{x}(t) - \dot{y}(t))^2 \tag{13}$$

(where C_{PTO} is the PTO damper coefficient) and considering that the sum of two jointly Gaussian variables is itself a Gaussian variable (see [13]), if we denote by z the relative velocity variable

$$z(t) = \dot{x}(t) - \dot{y}(t) \tag{14}$$

we may say that $z(t)$ is itself a Gaussian random variable with zero mean. Then the transfer function for the relative velocity may be expressed in terms of the transfer functions of the velocities of the two bodies and therefore of the hydrodynamic and mass coefficients of the system. Denoting by $h(t)$ the transfer function of $z(t)$ and by $\eta(t)$ the surface elevation, we have

$$z(t) = \eta(t) * h(t) = \int_{-\infty}^{\infty} \eta(t-\alpha) h(\alpha)\, d\alpha \tag{15}$$

in which the transfer function is possibly non-causal (see [9]). In the frequency domain we may write

$$z(\omega) = \eta(\omega) H(\omega) \tag{16}$$

where $H(\omega)$ is the Fourier Transform of $h(t)$ and $\omega = 2\pi f$ is the circular frequency (in rad/s). The function $H(\omega)$ is given by

$$H(\omega) = \frac{(D_y(\omega) - G(\omega))F_x(\omega) + (D_x(\omega) - G(\omega))F_y(\omega)}{D_x(\omega)D_y(\omega) - G(\omega)^2} \tag{17}$$

Here, $F_x(\omega)$ and $F_y(\omega)$ are the excitation force complex coefficients respectively for tube and piston, that may be obtained with the aid of a commercial BEM code (WAMIT), and the other terms (assuming the PTO coefficients C_{PTO} and K_{PTO} to be frequency-independent) are defined as

$$D_x(\omega) = j\omega(m_x + A_x(\omega)) + (B_x(\omega) + C_{PTO}) - \frac{j(K_{PTO} + \rho g S_W)}{\omega} \tag{18}$$

$$D_y(\omega) = j\omega(m_y + A_y(\omega)) + (B_y(\omega) + C_{PTO}) - \frac{j(K_{PTO})}{\omega} \tag{19}$$

$$G(\omega) = -j\omega A_{xy}(\omega) + (B_{xy}(\omega) + C_{PTO}) - \frac{j(K_{PTO})}{\omega} \tag{20}$$

Here, for each term on the right-hand-side, the subscript refers to the body considered (i.e. x correspond to the buoy + tube body, y to the piston and xy to cross-coupled terms) and m, A, B are respectively mass, added mass and radiation resistance terms. The term $\rho g S_{\mathrm{w}}$ represents the hydrostatic term due to the presence of a floating buoy (ρ is the water density, g the gravity acceleration and S_{w} is the buoy cross-sectional area defined by the undisturbed water free-surface).

We find that the variance of $z(t)$ is given by

$$\sigma_z^{\,2} = \int_0^{\infty} E(\omega)\left|H(\omega)\right|^2 d\omega = \int_0^{\infty} E(f)\left|H(f)\right|^2 df \tag{21}$$

where $E(f)$ is the energy spectrum of the sea-state. Now following again Papoulis ([13]), we may find that the average power is given by

$$\overline{P} = C_{PTO}\sigma_z^{\,2} \tag{22}$$

It follows from Eq. (21) and (22) that, considering the surface elevation as a stochastic input (represented by the spectrum $E(f)$), the PTF may be defined by

$$PTF(f) = C_{PTO}\left|H(f)\right|^2 \tag{23}$$

This means that the power average is given by the integral of the PTF times the spectrum considered. If we assume, for instance, a Dirac impulse centered on a certain

frequency f_e as input, we obtain the same results that could be found by applying a frequency domain analysis and that would correspond to the average power produced at that frequency.

For fixed device geometry, the PTF is only dependent on the values of the PTO coefficients, whose modification could imply different peak frequencies or shapes.

In the following we assume a device composed by a cylindrical buoy of radius 5m and draft 2.5m, a tube of 5m internal radius, 5.5m external radius 5.5m and 10m high. The piston is a disc of 5m radius and 0.5m thickness. These dimensions do not result from an optimization procedure, a step that would be important in device development but beyond the scope of this study.

Figure 3 shows four PTF for this particular geometry, plotted against the frequency, each one corresponding to a different PTO configuration (called IPS1, 2, 3 and 4).

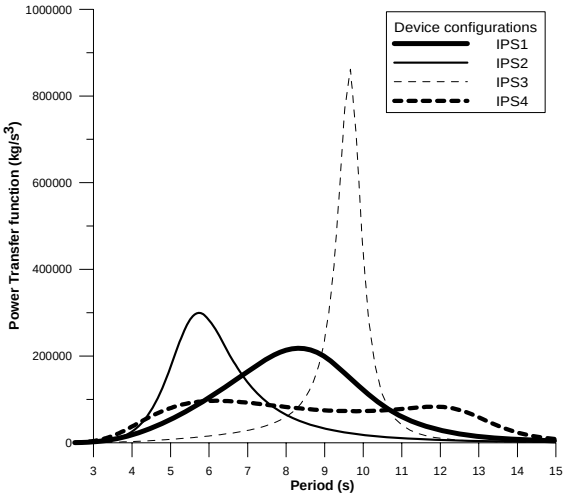

Figure 3: Power Transfer Functions of four linear PTO configurations (IPS1 to 4).

To achieve the objective of our study and observe the sensitivity to different bandwidth parameters, we name here χ_P as the capture width defined by the ratio between the average absorbed power and the incident wave power P_w

$$\chi_P = \frac{\overline{P}}{P_W} \tag{24}$$

4 Sensitivity of Capture Width to Spectral Bandwidth

The capture width χ_P of the converter has been defined in last section in such a way it is not influenced by the wave energy content (i.e. the variance m_0). Thus, the only influent parameters following the characterisation we proposed are the energy period T_{-10} and the spectral bandwidth (characterising the shape of the spectrum). It is then interesting to observe the distribution of χ_P against T_{-10} for each PTO configuration and each wave climate. This distribution over the energy period is obtained by considering the results output from the stochastic model for each spectral sub-sample, for which T_{-10} is fixed. Figures A1 to A8 (see end of paper) depict the average value of χ_P as well as its 90% confidence limits. The results obtained with Bretschneider spectra (defined in section 5) are also plotted. The same kind of patterns is observed in both wave climates when comparing each PTO configuration side-by-side. The slight differences in the amplitude of χ_P between the two locations may be explained by the fact some device configurations are more appropriate to a location or to another (i.e. IPS3 for FF and IPS2 for K13), as well as the fact the wave power in finite water depth is larger than in deep water, which makes χ_P lower. These figures clearly suggest that the spectral shape has a non-negligible impact on capture width. In particular, large variations of χ_P are observed in both wave climates when T_{-10} lies in the response band of the device. This is due to the fact that when the spectrum matches the device's pass-band, the spectral shape variations have much more influence in the integral of Eq. (21) than when they do not overlap completely. This implies that if a WEC is tuned to the sea-state, its performance may be greatly correlated with the spectral shape (or bandwidth). This point is more specifically addressed in the following.

When looking at the capture width obtained using Bretschneider spectra, an overestimation of χ_P is always noticed compared to the average value. This means that modelling sea-states with unimodal analytical spectra whose bandwidth is fixed (like a Bretschneider) when assessing the long-term performance assessment of a device may often result in very optimistic predictions. This issue is discussed more explicitly in next section.

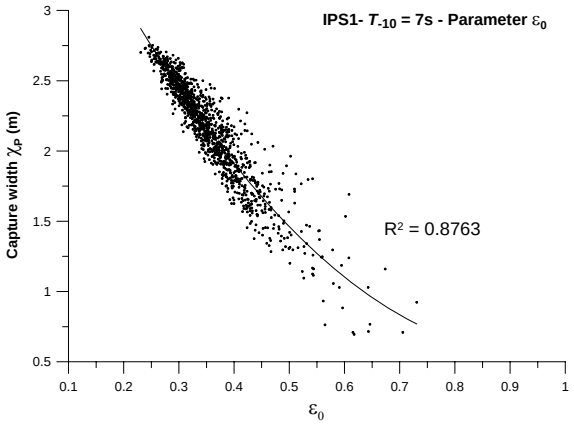

Figure 4: Scatter plot of capture width χ_P against parameter ε_0 for T_{-10} = 7s and PTO configuration IPS1 at FF.

In order to assess the ability of each bandwidth parameter in characterising the capture width when period T_{-10} is fixed, the distribution of χ_P against each parameter $\{\varepsilon_0, \varepsilon_1, \varepsilon_2, Q_p, \kappa, B_w\}$ is plotted for each PTO configuration, for each spectral sub-sample of each location. Then, it is fitted with a quadratic law by least squares method. The coefficient of determination R^2 of the trend is calculated and used as an indicator of the goodness of fit. If R^2 is close to 1, this means that the scatter plot follows the quadratic

trend well, or, in other words, that the capture width variations are well correlated to the bandwidth parameter's ones. Conversely, if R^2 is low, the points are too much scattered and no clear relationship linking the parameter to the capture width is observed. Figure 4 above gives the scatter plot of χ_P against parameter ε_0 obtained for configuration IPS1 and energy spectra of FF sub-sample T_{-10} = 7s. In this precise case the points are nicely fitted by the quadratic trend and a high value of R^2 is therefore found (~0.88).

Figures A9 to A16 (see end of paper) show the variations of coefficient R^2 against T_{-10} for each bandwidth parameter, PTO configuration and location. The average extracted power per period band is also plotted to indicate where the power production is the most significant (red spots). All the graphics have been set the same abscissas interval [3s;15s] in order to enable comparisons between both locations. To facilitate the interpretation of these results, we arbitrarily state that the correlation is good as soon as $R^2 > 0.70$. Thus, by looking at the four device configurations it is clear that some bandwidth parameters lead to better results than others, namely ε_0, ε_1, and B_w. A good relationship with capture width is found in particular over intervals of T_{-10} that match the pass-band of the devices (cf. Fig. 3). This can be observed at both locations as a fair correspondence appears between both sets of graphics in spite of the climatologic differences. For example, parameter ε_0 characterises capture width well for device configuration IPS1 over [5s;9s] at both FF and K13. Parameter κ, however, seems to perform better over intervals of periods that do not correspond to the converter's pass-band and which are systematically higher. In Figure A9 indeed, $R^2 > 0.70$ for κ when $T_{-10} \in$ [12s;15s]. Another important point to emphasize is the link between the interval of relevance of the parameters and the device's PTF broadness (or peakedness). Two extreme cases are exemplified through configurations IPS3 and IPS4. IPS3 refers to a very narrow-banded system with large response amplitude at resonance within [8s;11s], whereas IPS4 has a very low and wide pass-band that does not privilege any particular period within [4s;14s]. Figures A13 and A14 show that the parameters cannot characterise the capture width of device IPS3 over a wide interval of period. On the contrary, Figures A15 and A16 exhibit wide intervals of reliability, especially for parameters ε_0, ε_1, and B_w. The same properties can be also observed on configurations IPS1 and IPS2 as the first one of both corresponds to a broader PTF than the second one. Thus, it can be said that the broader the WEC's transfer function, the more sensitive the performance (here, the capture width) to spectral bandwidth. A practical conclusion of this point is that if a WEC (with vertical axisymmetry) is tuned to the most energetic period of the sea-states and provided its PTFs are not too narrow, the output power can always be characterised using a bandwidth parameter such as ε_0, ε_1, or B_w.

The use of parameters ε_2, Q_p and κ cannot be recommended as their respective performances are low, and/or highly dependent on the device configuration and the wave climate, as Figures A9 to A16 notably suggest.

5 Long-Term Performance Prediction

An investigation is made about the refinement of long-term WEC performance predictions by introducing spectral bandwidth in wave resource statistics. Indeed, comparing such results to actual values as well as those obtained by modelling the sea-states with analytical spectra is of particular interest. This is the objective of the present section, which deals with annual performance values in MWh.

The amount of extracted wave energy over one year at a given location is estimated by computing the power output (in kW) of the WEC on each sea-state spectrum and multiplying it by the time factor (in operating hours) of occurrence of this particular sea-state (characterised by H_{m0}, T_{-10}, …) within a whole year (that is, 365*24h = 8760h). As the real spectra of a given climate observed along one year represent a large amount of data, when available, and in order to simplify the estimation procedure, wave resource statistics and spectral models are more preferably used, as scatter tables of joint mean wave height and period occurrences and representative Bretschneider or JONSWAP spectra for example. If the percentage of occurrence is given as η%, the time factor is therefore 365*24*(η/100). In case the exact amount of converted energy has to be computed from a long-term sample of spectra (as here at FF and K13) then for each one of them $\eta/100 = 1/N_{sp}$ where N_{sp} is the total number of spectra in the sample, assuming the recorded sea-state occurrences are regularly spaced in time (which is the case for a "homogeneous" sample). Following this procedure, the exact annual extracted wave energy by each device configuration is calculated at both locations. The whole samples of respectively ~25300 and ~23000 energy spectral densities for FF and K13 are input in the model to this aim. The results (in MWh) are denoted by E_{ex}. Then, for each wave climate, an estimation based on Bretschneider spectra and scatter tables of joint (H_{m0},T_{-10}) occurrences is performed. The width of the H_{m0} and T_{-10} bins is 0.5m and 1s respectively, in order to work with a rather fine description of the wave climate. The partition of the rows and columns is crucial indeed, because the central H_{m0} and T_{-10} values of the cell are used to model the representative spectrum. Thus, the finer the table, the better the estimation. This procedure is the most common to date for WEC developers and designers, and the Bretschneider (or Pierson-Moskowitz) spectrum one of the most popular. This figure is called E_{Bret}.

A refined way of assessing annual WEC performance is proposed here by using 3D scatter tables, namely providing the (H_{m0},T_{-10},λ) occurrences where $\lambda \in \{\varepsilon_0, \varepsilon_1, B_w\}$. Only parameters ε_0, ε_1, and B_w have been retained for this study in regard to the conclusions drawn from previous section. The same procedure as using 2D scatter tables and Bretschneider spectra is carried out, adding one dimension – the spectral width – to the tables and considering a 3-parameter spectral model. These spectra (called here "Q_p-spectra") are a generalisation of the Bretschneider one, and can be expressed as

$$E(f) = \frac{H_{m0}^{\ 2}}{16} T_p \left(1 + 2Q_p\right) \frac{e^{-\alpha\left(fT_p\right)^{-2Q_p}}}{\left(fT_p\right)^{1+2Q_p}} \tag{25}$$

where $\alpha = 1 + 1/(2Q_p)$ and T_p is the spectrum's peak period, computed as

$$T_p = T_{-10} \frac{\alpha^{\alpha-1}}{\Gamma(\alpha)} \tag{26}$$

where $\Gamma(.)$ denotes the Gamma function. $Q_p = 2$ yields the Bretschneider spectrum. Thus, from the knowledge of H_{m0}, T_{-10} and Q_p, a unimodal spectral shape can be obtained for which spectral shape is controlled. Figure 5 depicts an example of such spectra for various values of factor Q_p, along with a typical JONSWAP 3.3 spectrum (for which $Q_p \sim 3.145$).

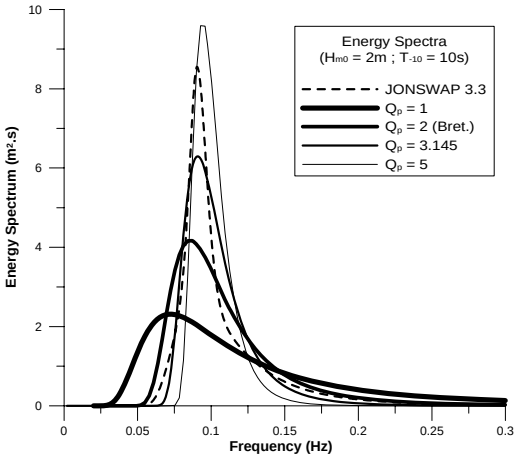

Figure 5: Plots of four Q_p-spectra (Q_p = 1, 2, 3.145 and 5) and JONSWAP 3.3 spectrum; for all, H_{m0} = 2m and T_{-10} = 10s.

In the previous section, the scatter plots of capture width χ_P against each bandwidth parameter were observed, and the results obtained using Q_p-spectra were superimposed to the clouds of points (i.e. for a large range of Q_p values, χ_P and the bandwidth parameters were computed on the theoretical spectra). A good agreement has been mostly found, so that the assumption that the Q_p-spectra reasonably follow the same general trends has been made. An example is shown on Figure 6 for IPS4 at FF (T_{-10} = 7.5s) against parameter ε_1. Although peakedness factor Q_p is not regarded as a relevant parameter for real spectra, it is regarded here as a shape factor for analytical spectrum.

Better estimations than E_{Bret} are expected for the annual converted wave energy by the device, since a refinement – the spectral bandwidth – has been introduced in the assessment procedure. 3D scatter tables are therefore built with the same H_{m0} and T_{-10} partitions as previously. Parameters ε_0 and ε_1 are partitioned in 0.1-wide bins and B_w in 0.025-wide. In each cell, the central values of H_{m0}, T_{-10} and λ parameterise the representative Q_p-spectrum of the cell which is input in the model. The value of Q_p that matches the central λ of the cell is found by dichotomy algorithm. The results obtained with parameters ε_0, ε_1 and B_w as third dimension of the sea-state description are respectively denoted by E_{Eps0}, E_{Eps1} and E_{Bw}.

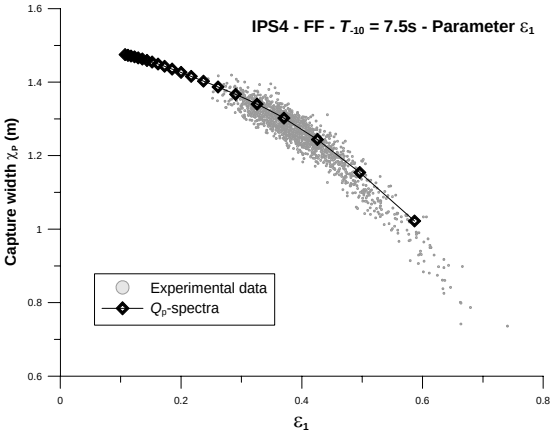

Figure 6: Scatter plot of capture width χ_P against ε_1 for T_{-10} = 7.5s and PTO configuration IPS4 from experimental data (FF) and analytical Q_p-spectra.

A last estimation method can be applied for FF thanks to the deep water assumptions, by considering the curves in Fig. A1 to A8. The central wave power P_w (Eq. (5)) is computed in each cell of the (H_{m0},T_{-10}) scatter table, and, assuming the independence of capture width on wave height, a semi-empirical power matrix is therefore easily obtained. The annual performance estimated by this way is denoted E_{KhiP}.

Tables 1 and 2 give the results of all these estimative procedures (in % of error with E_{Ex} given in MWh) obtained for the four PTO configurations at FF and K13.

FF	IPS1	IPS2	IPS3	IPS4
E_{Ex}	***251.4***	***156.4***	***266.6***	***193.1***
E_{Bret}	12.4%	5.2%	18.8%	4.8%
E_{KhiP}	-2.4%	-5.5%	0.9%	-0.8%
E_{Eps0}	5.8%	2.6%	10.7%	1.2%
E_{Eps1}	6.7%	6.2%	9.7%	1.1%
E_{Bw}	1.3%	5.9%	1.5%	-2.6%

Table 1: Performance predictions at FF (in % error against E_{Ex} in MWh/y)

K13	IPS1	IPS2	IPS3	IPS4
E_{Ex}	***177.7***	***194.6***	***89.4***	***119.8***
E_{Bret}	1.4%	-0.5%	26.4%	1.2%
E_{Eps0}	-1.2%	-4.5%	24.5%	-1.4%
E_{Eps1}	0.1%	-0.1%	21.3%	0.8%
E_{Bw}	9.0%	13.1%	9.8%	7.1%

Table 2: Performance predictions at K13 (in % error against E_{Ex} in MWh/y)

A first look at these tables first allows justifying the fact configuration IPS2 is more appropriate to the wave climate

at K13 (E_{Ex}). Then, confirming that the results of the narrow-banded configuration IPS3 cannot be satisfactorily predicted using spectral models since a substantial error is generally found (except 1.5% for E_{Bw} at FF). The only way of approaching the exact value with sufficient accuracy seems to be using the mean capture width χ_P obtained in realistic sea-states (0.9% for E_{KhiP} at FF only). It also confirms that predictions E_{Eps0} and E_{Eps1} for the broad-banded configuration IPS4 are quite precise at both locations (error < 2%). Parameter B_w yields more unstable results however (-2.6% at FF but 7.1% at K13).

Predictions based on Bretschneider spectra at FF lead to systematic overestimated performance values E_{Bret}. The method is therefore shown to be inconsistent for North-Atlantic locations such as the Portuguese coast. On the other hand, a nice accuracy is obtained at K13 with E_{Bret}, what clearly indicates that modelling North Sea sea-states by wind-waves spectra for assessing WEC performance is relevant. Even though – out of configuration IPS3 – E_{Eps1} and E_{Eps0} are also good estimates of E_{Ex}, their computation (heavier than E_{Bret}) may be useless at K13.

6 Conclusions

This study allowed observing the influence of spectral bandwidth of sea-states on the wave energy conversion operated by an axisymmetrical device equipped with a linear PTO, by considering several PTO configurations and two different wave climates. The results have shown that:

1 – The performance (here, the capture width χ_P) is highly sensitive to spectral shape variations within the pass-band of the device (Fig. A1 to A8);

2 – The broader the Power Transfer Function, the more the performance can be characterised by a spectral bandwidth parameter as ε_0, ε_1, or B_w within the device's response period interval (Fig. A9 to A16);

3 – Modelling sea-states by shape-fixed analytical spectra like a Bretschneider for long-term WEC performance assessment makes sense in the North-Sea where wind-waves are mostly expected; however, this may result in very erroneous (and overestimated) predictions in swell-dominated oceanic areas such as the North-Atlantic Ocean;

4 – The performance of narrow-banded WECs cannot be accurately assessed by considering analytical spectral shapes; estimator E_{KhiP} may be much more efficient in this case (under deep water and linearity assumptions for the model);

5 – If a WEC is able to tune to the most energetic period range of the sea-state, and provided the PTFs are not too narrow, the sensitivity to spectral bandwidth will be always ensured. In that case, estimators as E_{Eps0} and E_{Eps1} may result in very accurate long-term performance predictions (other specific shape-controlled analytical energy spectra may also be envisioned according to the location).

Acknowledgements

This work has been realized within the EC WAVETRAIN Research Training Network Towards Competitive Ocean Energy, contract n° MRTN-CT-2004-50166. The authors thank the *Rijkswaterstaat* for the use of the spectral wave data at K13. Co-authors PR and AF acknowledge the support of IDMEC through POCI2010 and FCT through contract nº POCTI/ENR/56079/2004.

References

[1] K. Hasselmann, et al. *Measurements of Wind-Wave Growth and Swell Decay During the Joint North Sea Wave Project (JONSWAP)*. Deutsche Hydr. Zeit, A (8º), 12, 1973.

[2] Y. Goda. *Random Seas and Design of Maritime Structures*. University of Tokyo Press, Japan, 1985.

[3] M. S. Longuet-Higgins. *Statistical Properties of Wave Groups in a Random Sea State*. Phil. Trans. R. Soc. Lond. A, 312, 219-250, 1984.

[4] D. Mollison. *Wave Climate and the Wave Power Resource*. Hydrod. of Ocean-Wave Energy Utilization, Proc. IUTAM Symp., Evans and Falcão (eds.), 133-156, Lisbon, Portugal, 1985.

[5] G. H. Smith, V. Venugopal, and J. Fasham. *Wave Spectral Bandwidth as a Measure of Available Wave Power*. In Proc. of Int. Conf. OMAE'06, Hamburg, Germany, 2006.

[6] Y. Goda. *On Wave Groups*. In Proc. of 1st Behaviour of Offshore Struct. Conf. '76, The Norwegian Institute of Technology, 1976.

[7] J. A. Battjes and G. P. van Vledder. *Verification of Kimura's Theory for Wave Group Statistics*. In Proc ICCE '84, 43, 642-648, 1984.

[8] D. V. Evans. *A Theory for Wave-Power Absorption by Oscillating Bodies*. J. Fluid. Mechanics, 77, 1, 1-25, 1976.

[9] J. Falnes. *Ocean Waves and Oscillating Systems: Linear Interactions Including Wave-Energy Extraction*. Cambridge University Press, Cambridge, UK, 2002.

[10] P. Ricci and A. F. de O. Falcão. *Wave Point Absorber Modelling*. In Proc. 9th World Renewable Energy Congress, WREN, Florence, 2006.

[11] A. F. De O. Falcão and R. J. A. Rodrigues. *Stochastic Modelling of OWC Power Plant Performance*. Applied Ocean Research, 24, 59-71, 2002.

[12] A. F. de O. Falcão. *Stochastic Modelling in Wave Power-Equipment Optimization: Maximum Energy Production Versus Maximum Profit*. Ocean Engineering, 31, 1407-1421, 2004.

[13] A. Papoulis**.** *Probability, Random Variables, and Stochastic Processes*. McGraw-Hill Series in Electrical Engineering, 1991.

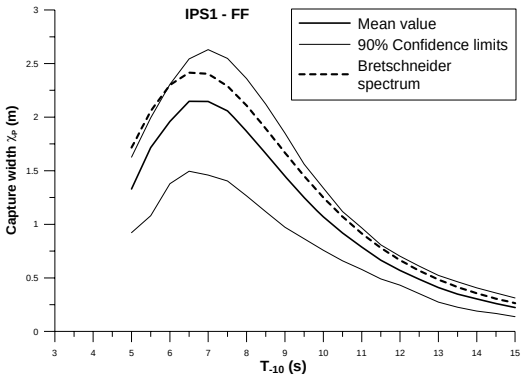

Figure A1: Distribution of χ_P against T_{-10} for IPS1 at FF; results for Bretschneider spectra.

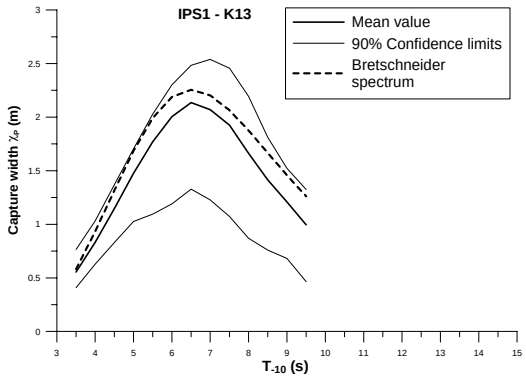

Figure A2: Distribution of χ_P against T_{-10} for IPS1 at K13; results for Bretschneider spectra.

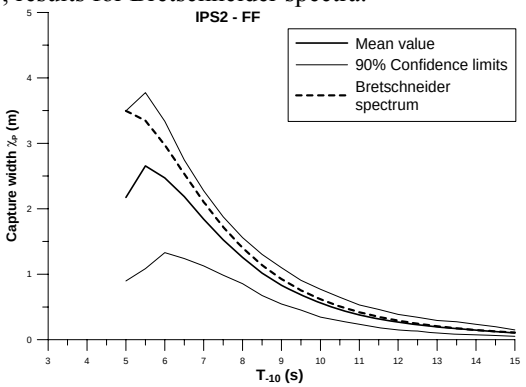

Figure A3: Id. Fig. A1 for IPS2.

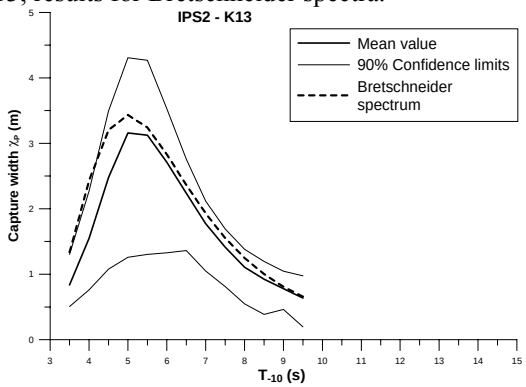

Figure A4: Id. Fig. A2 for IPS2.

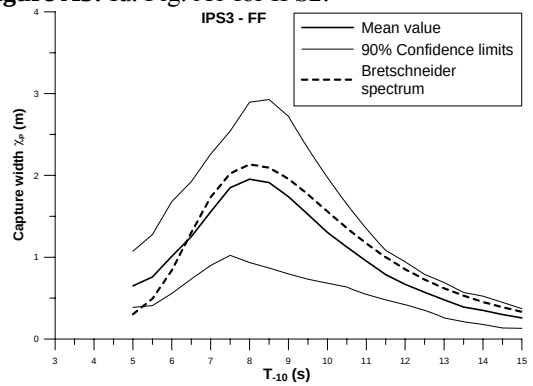

Figure A5: Id. Fig. A1 for IPS3.

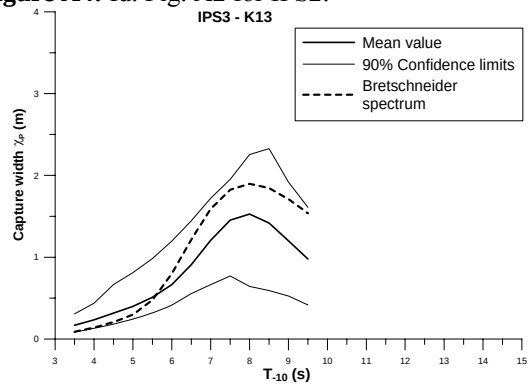

Figure A6: Id. Fig. A2 for IPS3.

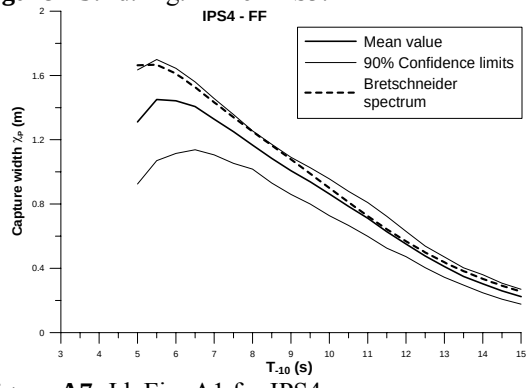

Figure A7: Id. Fig. A1 for IPS4.

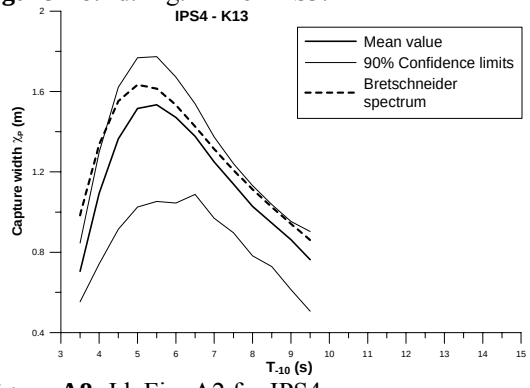

Figure A8: Id. Fig. A2 for IPS4.

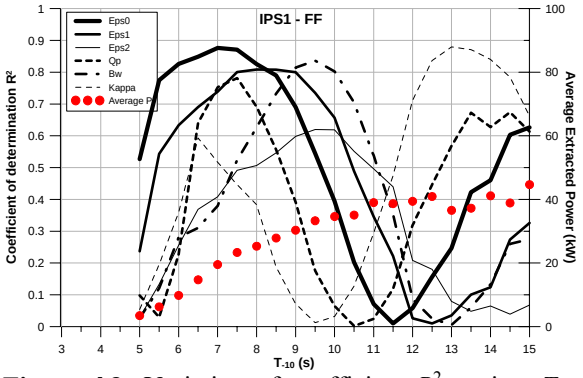

Figure A9: Variation of coefficient R^2 against T_{-10} for IPS1 at FF for each bandwidth parameter.

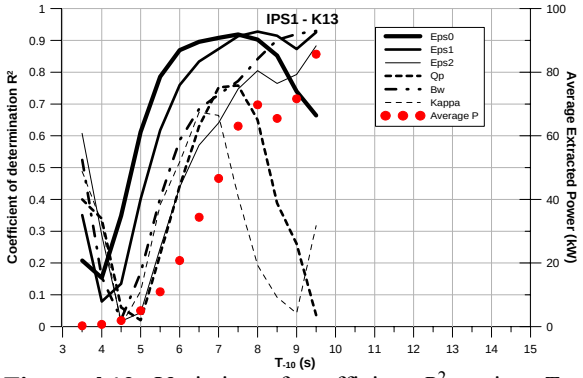

Figure A10: Variation of coefficient R^2 against T_{-10} for IPS1 at K13 for each bandwidth parameter.

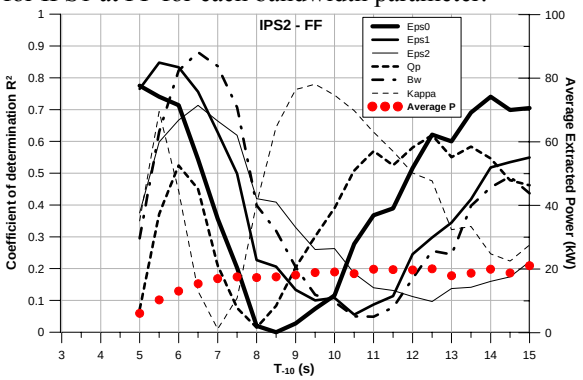

Figure A11: Id. Fig. A9 for IPS2.

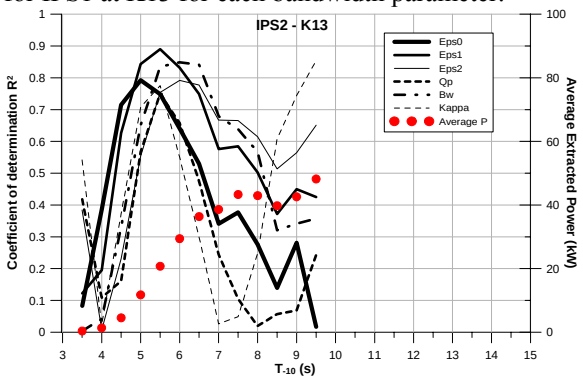

Figure A12: Id. Fig. A10 for IPS2.

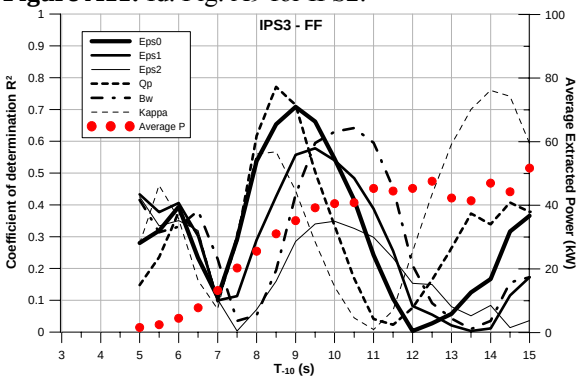

Figure A13: Id. Fig. A9 for IPS3.

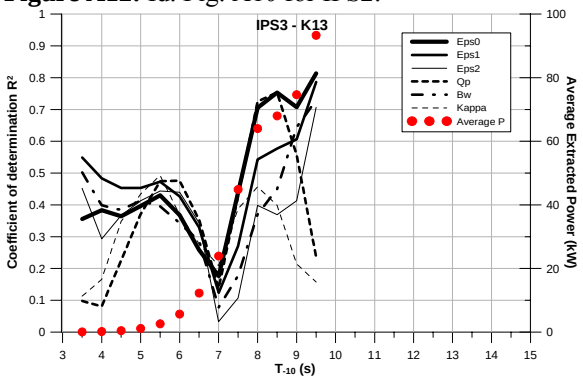

Figure A14: Id. Fig. A10 for IPS3.

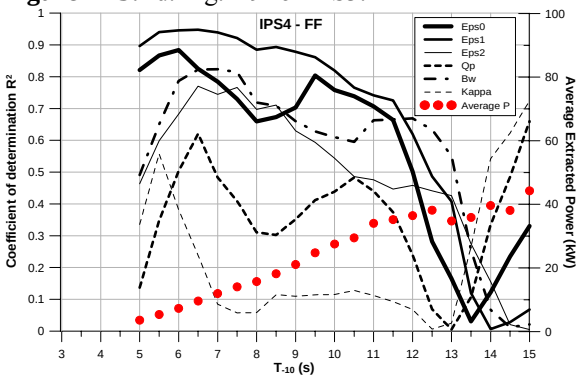

Figure A15: Id. Fig. A9 for IPS4.

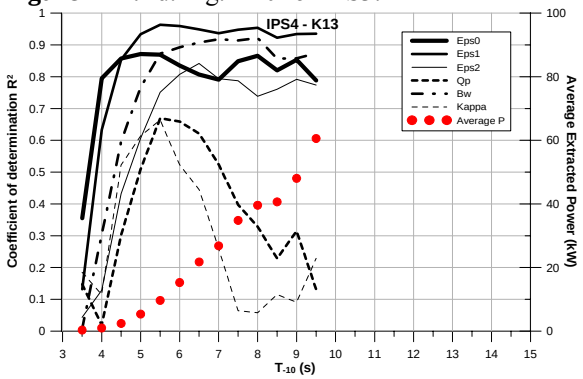

Figure A16: Id. Fig. A10 for IPS4.